2006

Worm algorithm and diagrammatic Monte Carlo: A new approach to continuous-space path integral Monte Carlo simulations

M Boninsegni

Nikolai Prokof'ev
University of Massachusetts - Amherst, prokofev@physics.umass.edu

Boris Svistunov
University of Massachusetts - Amherst, svistunov@physics.umass.edu

Worm Algorithm and Diagrammatic Monte Carlo: A New Approach to Continuous-Space Path Integral Monte Carlo Simulations

M. Boninsegni,[1] N.V. Prokof'ev,[2,3,4] and B.V. Svistunov[2,4]

[1] *Department of Physics, University of Alberta, Edmonton, Alberta T6G 2J1*
[2] *Department of Physics, University of Massachusetts, Amherst, MA 01003, USA*
[3] *BEC-INFM, Dipartimento di Fisica, Universita di Trento, Via Sommarive 14, I-38050 Povo, Italy*
[4] *Russian Research Center "Kurchatov Institute", 123182 Moscow, Russia*

A detailed description is provided of a new Worm Algorithm, enabling the accurate computation of thermodynamic properties of quantum many-body systems in continuous space, at finite temperature. The algorithm is formulated within the general Path Integral Monte Carlo (PIMC) scheme, but also allows one to perform quantum simulations in the grand canonical ensemble, as well as to compute off-diagonal imaginary-time correlation functions, such as the Matsubara Green function, simultaneously with diagonal observables. Another important innovation consists of the expansion of the attractive part of the pairwise potential energy into elementary (diagrammatic) contributions, which are then statistically sampled. This affords a complete microscopic account of the long-range part of the potential energy, while keeping the computational complexity of all updates independent of the size of the simulated system. The computational scheme allows for efficient calculations of the superfluid fraction and off-diagonal correlations in space-time, for system sizes which are orders of magnitude larger than those accessible to conventional PIMC. We present illustrative results for the superfluid transition in bulk liquid ^{4}He in two and three dimensions, as well as the calculation of the chemical potential of *hcp* ^{4}He.

PACS numbers: 75.10.Jm, 05.30.Jp, 67.40.Kh, 74.25.Dw

I. INTRODUCTION

It is now twenty years since Ceperley and Pollock (CP) carried out the first Path Integral Monte Carlo (PIMC) simulation of the superfluid transition of liquid ^{4}He.[1] Albeit restricted to a system of 64 ^{4}He atoms with periodic boundary conditions, that study demonstrated the feasibility of *ab initio* numerical studies of quantum many-body systems, the mass of the particles and the interaction potential being the sole input to the calculation.

The PIMC method, in the form developed by CP (henceforth referred to as "conventional"), has since played a major role in the theoretical investigation of quantum many-body systems. Not only has it provided quantitative results for a wide range of physical systems, it has also shaped, to some extent, our qualitative understanding of such phenomena as superfluidity (SF) and Bose condensation, at the microscopic level. At least for Bose systems, PIMC is the *only* presently known method capable of furnishing in principle *exact* numerical estimates of physical observables at finite temperature (T), including the superfluid (ρ_s) and condensate ($n_\circ$) fractions. Moreover, despite the notorious *sign* problem, that has so far made it impossible to obtain equally high quality results for Fermi systems, PIMC proves a valid option in this case as well, allowing one to obtain approximate estimates of accuracy at least comparable to that afforded by the other leading methods.[2,3]

It thus seems reasonable to regard PIMC as a realistic option to investigate ever more complex quantum many-body systems, and it makes sense to try and overcome its most important present limitations. Aside from the above-mentioned *sign* problem, which we do *not* discuss in this paper, the main bottleneck of the current PIMC technology is inarguably the maximum system size (i.e., number N of particles) for which accurate estimates can be obtained, in a reasonable amount of computer time. Specifically, the computational effort required to study properties that most directly depend on particle indistinguishability, is observed to scale prohibitively with N.

For example, the superfluid fraction ρ_s is obtained in a PIMC simulation of bulk condensed matter, by means of the so-called winding number estimator,[5] which can only take on a nonzero value if long permutation cycles of identical particles occur. In conventional PIMC, the frequency with which such cycles are sampled, is an *exponentially* decreasing function of N. For this reason, and in spite of (at least) a hundredfold increase in computer speed,[4] since the pioneering work of Ref. 1 it has not proven possible to obtain estimates of the superfluid fraction in bulk liquid ^{4}He for finite systems of more than N=64 particles. Besides the unfavorable scaling of computing resources as a function of N, another major issue that this entails is the difficulty of assessing reliably whether the observed absence of long permutation cycles reflects a genuine physical effect, or merely lack of ergodicity of the path sampling scheme.[6]

How important is the above size limitation ? For most observables diagonal in the coordinate representation, one can often approach surprisingly closely the thermodynamic limit by simulating as few as ~ 30 particles, especially for systems characterized by short-ranged, Lennard-Jones-type interactions. On the other hand, an accurate *quantitative* characterization of the superfluid transition (including the calculation of the transition temperature T_c) can only be obtained via finite-size

scaling analysis of results for $\rho_s(T)$ and/or $n_\circ(T)$. The reliability of this procedure crucially hinges on the availability of data for large systems of significantly different sizes. Attempts to estimate T_c for superfluid ^{4}He, based on PIMC data for $\rho_s(T)$ for systems of size N=64 and smaller, failed to yield quantitative results.[7]

But there are other reasons, arguably more important than the mere pursuit of numerical accuracy, pointing to the importance and timeliness of extending by one or two orders of magnitude the size of the systems accessible to PIMC. Quite generally, in order for a scientific question to be meaningfully addressed by numerical simulations, the size of the simulated system should be greater than all characteristic length scales affecting the physics of interest. This is particularly important in the study of inhomogeneous phases of matter, or fluids in confinement, or restricted geometries. An example is provided by the study of helium fluid in porous glass, such as Vycor; the diameter of a characteristic pore is of the order of a few tens of Å. Thus, a realistic calculation, at the typical liquid helium density, requires that one be able to simulate a system comprising several thousands of atoms. Other examples are the numerical investigations of multicomponent systems, as well as of grain boundaries, dislocations and other defects in quantum solids, or of incommensurate phases of films of helium or *para*-hydrogen adsorbed over substrates such as graphite.

Over the past two decades, there has been relatively little experimentation with approaches to PIMC simulations differing in some important aspects from the conventional one of CP, thoroughly described in Ref. 2. As mentioned above, in conventional PIMC the simulation of properties that are most directly affected by quantum statistics (i.e., by many-particle permutations), suffers from a very unfavorable scaling of required computer time with system size. This hurdle seems difficult to conquer within conventional PIMC, and more generally within any Monte Carlo scheme formulated in the canonical ensemble, in which the winding number becomes "topologically locked" in the $N \to \infty$ limit.[2]

On the other hand, the same hurdle has been completely overcome in Quantum Monte Carlo (QMC) simulations of lattice models. A lattice Path Integral scheme based on an alternative sampling approach, known as *worm algorithm* (WA),[8] has been demonstrated to allow for efficient calculations of winding numbers and of the one-particle Green function G, for systems of as many as $\sim 10^6$ particles.[9] It is particularly useful for the studies of critical phenomena since it does not suffer from the critical slowing down problem[10] present in other local-update schemes.

The WA has been recently extended to the study of systems in continuous space;[11] it has first been shown to afford the simulation of the superfluid transition in liquid ^{4}He in two dimensions, for systems comprising as many as 2500 particles, i.e., about 100 times greater than those accessible to conventional PIMC. Subsequently, it has been applied to the study of Bose condensation in crystalline ^{4}He,[12] as well as to the investigation of superfluid properties of *para*-Hydrogen droplets.[13]

In all of these applications, the WA has provided accurate numerical results, simply not obtainable with any other existing method. It need be stressed, however, that the WA is not merely about doing large system sizes (important as this is); it is also the first *grand canonical* QMC method with local updates to incorporate in full quantum statistics. It affords the exact computation of imaginary-time off-diagonal correlations, such as the one-particle Matsubara Green function, that are not accessible to conventional PIMC (nor to any other QMC technique in continuous space).

In this paper, we provide a detailed description of this new, powerful computational tool, which promises to open novel avenues to the theoretical exploration of strongly correlated many-body system. The manuscript is organized as follows: in the next section (II), we describe the simplest implementation of the WA, also introducing our nomenclature, configurational space and data structure. In section III, we discuss in detail the computation of the Matsubara Green function, as well as of its equal-time limit, namely the one-particle density matrix. In section IV, we describe an important enhancement of the simple implementation, namely the expansion of (the attractive part of) the potential energy of interaction among particles in elementary (diagrammatic) contributions, that are then sampled by a Monte Carlo method. This scheme, which falls in the general category of Diagrammatic Monte Carlo techniques,[14] allows for the full inclusion of the contribution of the potential energy (for an important class of potentials) at a computational cost that is *independent* of the size of the system.

In Sec. V, we provide some quantitative information related to the specific utilization of the WA in simulation studies of superfluid ^{4}He. In Sec. VI, we offer a quantitative demonstration of the power of the WA, by illustrating in detail our results for simulations of the superfluid transition of liquid ^{4}He in two and three dimensions. We outline our conclusions, and discuss outlook for future applications of the WA, in Sec. VII.

II. SIMPLEST VERSION

We begin with some basic notation. We assume for definiteness a system of identical particles (in d dimensions) obeying Bose statistics.[15] Let m be the mass of each particle. The system is enclosed in a cubic vessel of volume $V = L^d$, with periodic boundary conditions in all directions (other geometries, boundary conditions, and/or external forces require obvious and minimal modifications which are standard for any QMC scheme).

We make from the outset the assumption of working in the *grand canonical* ensemble; that is, the system is held in thermal equilibrium with a heat reservoir at temperature $T = 1/\beta$ (we set k_B=1), with which it can exchange particles as well. Consequently, in order to specify the

thermodynamic state of the system, we need to assign the chemical potential μ, which is an input parameter in our computational scheme, just like the temperature T. The number of particles N is allowed to fluctuate.

Let $\hat{H}$ be the (many-body) system Hamiltonian, which we assume of the following form:

$$\hat{H} = -\lambda \sum_{i=1}^{N} \nabla_i^2 + \sum_{i<j} v(|\mathbf{r}_i - \mathbf{r}_j|) \,, \tag{2.1}$$

where $\lambda = \hbar^2/2m$ and where v is a pairwise interaction potential that depends only of the relative distance between any two particles.[16] Below, R will always be used as a collective "coordinate", representing positions of all particles in the system, i.e., $R \equiv (\mathbf{r}_1, \mathbf{r}_2, \ldots, \mathbf{r}_N)$.

A. Configurational Space

A fundamental aspect of the WA, which crucially distinguishes it from conventional PIMC and from all existing QMC methods in the continuum, is that it operates in an extended configurational space, containing both closed world line configurations (henceforth referred to as Z- or diagonal configurations), as well as configurations containing one open world line (worm). The Z-configurations contribute to the partition function, whereas those with an open world line contribute to the one-particle Matsubara Green function; in the following, the latter will be referred to as G- (or, off-diagonal) configurations. As we shall see, all topologically non-trivial modifications of world lines occur in the off-diagonal configurational space (or, G-sector). The sampling process allows for transitions from the G- to the Z-sector (by closing, or removing the existing open world line) and vice versa (by creating a new open world line, or by opening an existing closed one). Expectation values of all physical quantities of interest (with the exception of the Green function), including particle and winding numbers, are only updated when the random walk generates a diagonal configuration.

Next, we proceed to describe in detail the two sectors in which our configuration space is conceptually divided.

1. The Z-sector

The Z-sector of our configuration space, is nothing but the full configuration space of conventional PIMC. It naturally emerges from the Path Integral representation of the grand partition function $Z = \mathrm{Tr}\, e^{-\beta \hat{K}}$, where $\hat{K} = \hat{H} - \mu \hat{N}$.

Each $Z-$*configuration* is a discrete imaginary-time many-particle path, $X \equiv (R_0, R_1, R_2, \ldots, R_P)$, with $R_P \equiv R_0$ (except for a possible permutation of particle labels), representing the integrand in the asymptotically exact (in the $P \to \infty$ limit) integral decomposition of Z

$$Z \approx \sum_{N=0}^{\infty} e^{\beta \mu N} \int dX \; A(X, \varepsilon)\, \mathrm{e}^{-U(X)} \,, \tag{2.2}$$

where $dX \equiv dR_0 dR_1 ... dR_{P-1}$, $\varepsilon = \beta/P$, and where

$$A(X, \epsilon) \equiv \prod_{j=0}^{P-1} \rho_F(R_j, R_{j+1}, \varepsilon) \,.$$

In turn, ρ_F is a product of free-particle imaginary-time propagators, i.e., with an obvious notation,

$$\rho_F(R_j, R_{j+1}, \epsilon) = \prod_{i=1}^{N} \rho_\circ(\mathbf{r}_{ij}, \mathbf{r}_{i,j+1}, \varepsilon) \tag{2.3}$$

with

$$\rho_\circ(\mathbf{r}, \mathbf{r}', \epsilon) = (4\pi\lambda\epsilon)^{-d/2} \exp\left[-\frac{(\mathbf{r} - \mathbf{r}')^2}{4\lambda\epsilon} \right] . \tag{2.4}$$

The function U in Eq. (2.2) incorporates correlations, both in space and in imaginary time, arising from interactions among particles. U is chosen so that, in the $\varepsilon \to 0$ limit, the distribution of discrete paths X will asymptotically approach the correct continuous limit. Several choices are possible[2] for U, but the simplest version of the algorithm described in this section does not depend on its particular form. In what follows, we refer to the product $W(X) \equiv A(X, \varepsilon)\ \mathrm{e}^{-U(X)}$ as a *configurational weight*.

Eq. (2.2) implies the following configuration space structure: one has N single-particle paths (world lines), labeled $i = 1, 2, \ldots, N$, propagating in the discretized imaginary time interval $[0, \beta]$ (specifically, $t_0 = 0$, $t_P = \beta$). Each world line consists of P successively linked "beads" (particle positions), labeled by the index of the corresponding imaginary time "slice", $j = 0, \ldots, P-1$. The j-th bead of the i-th world line is positioned at $\mathbf{r}_{ij}$.

As a result of β-periodicity, coupled with the physical indistinguishability of particles, the $(P-1)$-st bead of each world line must be linked to the zero-th bead of either the same, or another world line. For both theoretical and practical (data structure) purposes, it is advantageous to guarantee β-periodicity automatically; to this aim, we regard world line configurations as closed loops on a $(d+1)$-dimensional surface of a $(d+2)$-dimensional β-cylinder, on which lie P equidistant (and equivalent) imaginary time "hyperplanes" (corresponding to the different time slices), labelled $j = 0, \ldots, P-1$. It should be noted that the total number of world line loops defined on the β-cylinder can be different from the total number of particles; this is because a single world line which "winds around" the imaginary time interval l times before returning to its initial position represents not just one particle, but rather l particles involved in the same exchange cycle. The presence of such exchange cycles is essential, in order to incorporate in the computational scheme the symmetry of the system with respect to particle permutations.

2. The G-sector

The G-sector of our configurational space comes from the representation—analogous to that of the partition function, Eq. (2.2)—of the one-particle Matsubara Green function

$$G(\mathbf{r}_1,\mathbf{r}_2,\tau) \;=\; \langle\, \mathcal{T}\{\hat{\psi}(\mathbf{r}_1,\tau)\;\hat{\psi}^\dagger(\mathbf{r}_2,0)\}\,\rangle \;\equiv\; \frac{g(\mathbf{r}_1,\mathbf{r}_2,\tau)}{Z}\;, \tag{2.5}$$

where $\langle\ldots\rangle$ denotes thermal averaging, $\mathcal{T}$ is the time-ordering operator and $\hat{\psi}^\dagger(\mathbf{r},\tau)$ and $\hat{\psi}(\mathbf{r},\tau)$ are (Bose) particle creation and annihilation operators in Matsubara representation. The structure of the integral representation of $g(\mathbf{r}_1,\mathbf{r}_2,\tau)$ is very similar to that of Z. In fact, the only qualitative difference of a G-sector ("off-diagonal") configuration from a diagonal one, is that the former contains a *worm*, that is, a world line on a β-cylinder with two ends—the "head" and the "tail"—corresponding to the Green function annihilation and creation operators, respectively. The two special beads at the open world line ends are named (for historical reasons) *Ira* ($\mathcal{I}$) and *Masha* ($\mathcal{M}$). Configurations in which $\mathcal{I}$ and $\mathcal{M}$ are located in space-time at points $(\mathbf{r}_\mathcal{I},\tau_\mathcal{I})$ and $(\mathbf{r}_\mathcal{M},\tau_\mathcal{M})$ contribute to $g(\mathbf{r}_\mathcal{I},\mathbf{r}_\mathcal{M},\tau_\mathcal{I}-\tau_\mathcal{M})$ with the weight defined in accordance with Eq. (2.2) generalized to include the off-diagonal configuration sector.

Formally, the ensemble of WA configurations corresponds to the generalized partition function

$$Z_W = Z + Z'\;, \tag{2.6}$$

with

$$Z' = C\sum_{j_\mathcal{I},j_\mathcal{M}}\int d\mathbf{r}_\mathcal{I}\;d\mathbf{r}_\mathcal{M}\;g(\mathbf{r}_\mathcal{I},\mathbf{r}_\mathcal{M},\,\varepsilon(j_\mathcal{I}-j_\mathcal{M}))\;. \tag{2.7}$$

The value of dimensionless parameter C only affects the efficiency of the simulation, as C controls the relative statistics of Z- and G-sectors; for the moment, we leave it undetermined, to come back to it later on, when discussing updates.

An important new feature that arises when going from Z to Z_W, is that the number of continuous variables in G-sector configurations is not constant, but rather varies from configuration to configuration. This immediately points to Diagrammatic Monte Carlo,[14] as a general way to perform updates whenever the number of variables to sample, is itself variable.

The sampling of paths $\{X_l\}$, is implemented within the WA *exclusively* through a set of simple, *local* space-time updates involving $\mathcal{I}$ (or, $\mathcal{M}$). The particle number becomes configuration- and time-dependent (there is one less particle between $\mathcal{I}$ and $\mathcal{M}$, than in the rest of the path). This clearly shows how, by its very construction, the WA opens up the possibility of working in the *grand canonical* ensemble, with the chemical potential μ being an input parameter.[17] Obviously, WA updates can be combined with the conventional PIMC updates to have the most flexible scheme.

In accordance with Eq. (2.7), the simplest estimators in WA are [assuming that configurations are sampled from the probability density $W(X)$]

$$\delta^{(Z)} \;=\; \begin{cases} 1\;, & \text{if in } Z\text{-sector}\;,\\ 0\;, & \text{if in } G\text{-sector}\;,\end{cases} \tag{2.8}$$

$$\delta^{(G)} \;=\; \begin{cases} 0\;, & \text{if in } Z\text{-sector}\;,\\ 1\;, & \text{if in } G\text{-sector}\;.\end{cases} \tag{2.9}$$

In the statistical limit, their Monte Carlo averages are

$$\langle\,\delta^{(Z)}\rangle_{\rm MC} \;=\; Z/Z_W\;, \tag{2.10}$$

$$\langle\,\delta^{(G)}\rangle_{\rm MC} \;=\; \frac{CP}{Z_W}\sum_{j=0}^{P-1}\int d\mathbf{r}_1\,d\mathbf{r}_2\;g(\mathbf{r}_1,\mathbf{r}_2,\varepsilon j)\;, \tag{2.11}$$

In particular

$$\frac{\langle\,\delta^{(G)}\rangle_{\rm MC}}{\langle\,\delta^{(Z)}\rangle_{\rm MC}} \;=\; CP\sum_{j=0}^{P-1}\int d\mathbf{r}_1\,d\mathbf{r}_2\;g(\mathbf{r}_1,\mathbf{r}_2,\varepsilon j)\;. \tag{2.12}$$

The simplest estimator for $g(\mathbf{r},\tau)$, $\tau=\varepsilon j$, is given by

$$\langle\,\delta^{(G)}\,\delta_{j,\,(j_\mathcal{I}-j_\mathcal{M})}\,\delta(\mathbf{r}_1-\mathbf{r}_\mathcal{I})\,\delta(\mathbf{r}_2-\mathbf{r}_\mathcal{M})\,\rangle_{\rm MC} \;=\; \;=\; \frac{CP}{Z_W}\,g(\mathbf{r}_1,\mathbf{r}_2,\varepsilon j)\;. \tag{2.13}$$

However, below we introduce a more elaborate scheme which allows one to circumvent the problem of working with generalized functions (typically solved by collecting statistics to finite-size spatial bins at the expense of an additional systematic error).

B. Data Structure and Updates

In this section, we describe a set of ergodic local updates which sample the extended configuration space, switching between the Z- and G-sectors. Updates which change the number of continuous variables in X, are arranged in complementary pairs, designed so as to satisfy the requirement of detailed balance. General principles of balancing complementary pairs can be found in Ref. 14. We have three pairs of updates altogether: *Open/Close*, *Insert/Remove*, and *Advance/Recede*. Only the *Swap* update in the list below does not fall in this category, because it preserves the number of variables, i.e., it is self-complementary. Proposed updates are either accepted or rejected based on the Metropolis algorithm, according to the standard procedure.[18]

In order to keep the presentation simple, the sampling scheme described below is one in which every update can be proposed, regardless of its applicability to the current configuration (for example, the proposal to *Remove* the worm is allowed even if there is no worm in the current configuration, in which case the proposed update will

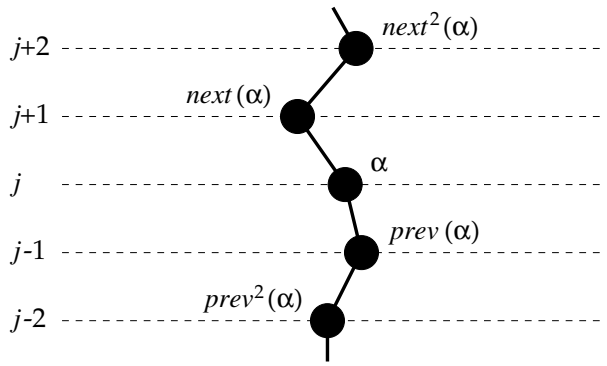

FIG. 1: World line beads on the β-cylinder and nearest neighbor associations between them.

necessarily be rejected). It should be understood, however, that standard sampling tricks can be used, whereby only applicable updates are proposed, thereby enhancing the performance.[19]

To be specific, let us adopt the following data structure: all beads are labeled, and each bead is linked to its two world-line neighbors, the *next* and the *previous* beads on the β-cylinder, see Fig. 1. It proves convenient to introduce two functions, '*next*' and '*prev*', mapping each bead onto its next and previous neighbor, respectively. Correspondingly, $\sigma = next^m(\alpha)$ means that the bead σ is the result of the m-fold application of '*next*' to the bead α; likewise, $\alpha = prev^m(\sigma)$.

In order to have an efficient spatial addressing of beads, and thus a scalable algorithm (i.e., one in which the number of operations required to perform updates does not depend on either system size, nor temperature), we use nearest-neighbor tables at all imaginary time slices.[20] That is, for each time slice, the volume of the system is hashed into equal microscopic "bins", labeled by the discrete time label, $j = 0, 1, 2, \ldots, (P-1)$, and discrete radius vector, $\vec{\mathcal{R}}$. [In practice, we set the bin volume, Ω, to be of the order of the volume per particle.] For each bin there is a list of all beads contained in it. Accordingly, addressing/searching relevant beads is performed through nearest-neighbor tables and next/previous links.

(1a) Open. The update is only possible if the configuration is diagonal. A bead α is selected at random. An integer number M is selected at random within the interval $[1, \bar{M}]$ with $\bar{M} < P$ being an arbitrary algorithm parameter. Then, $(M-1)$ beads, namely, $next^1(\alpha)$, $next^2(\alpha)$, $\ldots$, $next^{(M-1)}(\alpha)$ are removed, so that a worm appears with $\mathcal{I} = \alpha$ and $\mathcal{M} = \sigma \equiv next^M(\alpha)$. The acceptance probability for this update is

$$P_{\rm op} = \min\left\{1,\ \frac{C\,\bar{M}\,N_{\rm bd}\ {\rm e}^{\Delta U - \mu M\varepsilon}}{\rho_\circ(\mathbf{r}_\alpha, \mathbf{r}_\sigma, M\varepsilon)}\right\}, \qquad (2.14)$$

where $\Delta U = U(X) - U(X^\star)$ is the difference between the U-function values for the initial (X) and proposed $(X^\star)$ configurations, $N_{\rm bd}$ is the total number of beads in the initial diagonal configuration equal to the number of particles, N, times the number of slices, $N_{\rm bd} = NP$. If $M = 1$, then no beads are removed; only the link between the beads α and σ disappears with the appearance of $\mathcal{I}$ and $\mathcal{M}$.

(1b) Close. This update is only possible if the configuration is off-diagonal. Let the integer $M \geq 0$ be the discrete algebraic distance from $\mathcal{I}$ to $\mathcal{M}$, understood as a number of time-slice steps—in the *positive direction* on the β-cylinder—one has to make to reach the slice at which $\mathcal{M}$ is currently positioned, starting from that of $\mathcal{I}$. If $M > \bar{M}$ or $M = 0$, then the move is rejected,[19] otherwise, one proposes to generate a piece of world line connecting $\mathcal{I}$ to $\mathcal{M}$, thereby rendering the configuration diagonal. If $M > 1$, the corresponding spatial positions of new $(M-1)$ beads, $\mathbf{r}_1, \mathbf{r}_2 \ldots, \mathbf{r}_{M-1}$, are sampled from the product of M free-particle propagators $\prod_{\nu=1}^{M} \rho_\circ(\mathbf{r}_{\nu-1}, \mathbf{r}_\nu, \varepsilon)$, where $\mathbf{r}_0 \equiv \mathbf{r}_\mathcal{I}$ and $\mathbf{r}_M \equiv \mathbf{r}_\mathcal{M}$. The probability of accepting the move is

$$P_{\rm cl} = \min\left\{1,\ \frac{\rho_\circ(\mathbf{r}_\mathcal{I}, \mathbf{r}_\mathcal{M}, M\varepsilon)\ {\rm e}^{\Delta U + \mu M\varepsilon}}{C\,\bar{M}\,N_{\rm bd}}\right\}, \qquad (2.15)$$

where N_{bd} is the number of beads in the final diagonal configuration. In our implementation, proposed *Open* and *Close* updates are automatically rejected whenever the quantity

$$\frac{(\mathbf{r}_\mathcal{I} - \mathbf{r}_\mathcal{M})^2}{4M\lambda\epsilon}$$

is larger than some (arbitrary) number of order unity, so as to avoid small acceptance ratios in the close update when the worm ends are far away in space (in our simulations we set this number equal to 4).

(2a) Insert. The other way to create an off-diagonal configuration from a diagonal one, besides *Open*, is to seed a new, M-link long, open world line. The number of links $1 \leq M \leq \bar{M}$ and the position of $\mathcal{M}$ in space-time are selected at random. The spatial positions of the other M beads are generated from the product of M free-particle propagators. The move is accepted with probability

$$P_{\rm in} = \min\{1,\ C\,V\,P\,\bar{M}\,{\rm e}^{\Delta U + \mu M\varepsilon}\}\,, \qquad (2.16)$$

where V is the volume of the system, as mentioned above.

(2b) Remove. The removal of the worm, i.e., of the world line connecting $\mathcal{M}$ to $\mathcal{I}$, is proposed, provided its algebraic length is $1 \leq M \leq \bar{M}$. (If $M > \bar{M}$, the proposal is rejected.[19]) The acceptance probability for the move is

$$P_{\rm rm} = \min\{1,\ {\rm e}^{\Delta U - \mu M\varepsilon}/CVP\,\bar{M}\}\,. \qquad (2.17)$$

At this point, we are in position to discuss the value of the constant C, which up to now we have left undetermined. A natural choice is

$$C = C_0/VP\,\bar{M}\,, \quad C_0 \sim O(1)\,, \qquad (2.18)$$

so that the probabilities to *Open*, *Close*, *Insert*, or *Remove* a worm, do not contain macroscopically large/small factors, and are of order unity at the optimal choice of $\bar{M}$. Normally, optimal $\bar{M}$ is such that the time $\varepsilon\bar{M}$ is of the order of the characteristic single-particle time, which guarantees that the exponentials in the acceptance probabilities are of order unity, while the propagators are of the order of the particle number density. This implies the following scaling:

$$C \propto \frac{\varepsilon^2}{V\beta} . \tag{2.19}$$

(3a) Advance. This move advances $\mathcal{I}$ by a random number M of slices forward in time. Its implementation is similar to that of *Insert*. The acceptance probability is

$$P_{\rm ad} = \min\{1,\, {\rm e}^{\Delta U + \mu M\varepsilon}\} \tag{2.20}$$

(3b) Recede. Now $\mathcal{I}$ is displaced backwards in time (again, in a β-periodic sense), by erasing M consecutive links; the number $1 \le M \le \bar{M}$ is selected at random. The acceptance probability is

$$P_{\rm re} = \min\{1,\, {\rm e}^{\Delta U - \mu M\varepsilon}\} \tag{2.21}$$

If M turns out to be equal to or larger than the number of links in the worm, the update is rejected.[19]

(4) Swap. This update is applicable to off-diagonal configurations only and is illustrated in Fig. 2. Let $\mathcal{I}$ be positioned on the j-th slice in the bin $(\vec{\mathcal{R}}_{\mathcal{I}}, j)$. Consider the $(j+\bar{M})$-th slice (because of β-periodicity, this addition is understood modulo P) and create a temporary list, $\mathcal{L}_{\mathcal{I}}$, of all the beads that are contained, at the slice $j+\bar{M}$, in the bins that spatially coincide with the bin $(\vec{\mathcal{R}}_{\mathcal{I}}, j)$ or with one of its nearest neighbors.[21] Select one bead, α, from the list, with the probability

$$T_\alpha \;=\; \rho_\circ(\mathbf{r}_{\mathcal{I}}, \mathbf{r}_\alpha, \bar{M}\varepsilon)/\Sigma_{\mathcal{I}} \;, \tag{2.22}$$

where

$$\Sigma_{\mathcal{I}} \;=\; \sum_{\sigma\in\mathcal{L}_{\mathcal{I}}} \rho_\circ(\mathbf{r}_{\mathcal{I}}, \mathbf{r}_\sigma, \bar{M}\varepsilon) \tag{2.23}$$

is the normalization factor. If any of the beads α, $prev^1(\alpha)$, $prev^2(\alpha)$, ..., $prev^{\bar{M}}(\alpha)$ coincides with $\mathcal{M}$, the move is rejected. Next, consider the bead $\zeta = prev^{\bar{M}}(\alpha)$ and identify its bin, $(\vec{\mathcal{R}}_\zeta, j)$. One must now check whether the bead α is contained in the bin spatially coinciding with $(\vec{\mathcal{R}}_\zeta, j)$, or with one of its nearest neighbors; if that is not the case, the move is rejected. A second list is then created, $\mathcal{L}_\zeta$, of beads contained in the $(\vec{\mathcal{R}}_\zeta, j+\bar{M})$ bin and in its nearest neighboring ones. At this point, a set of new positions between beads α and $\mathcal{I}$ is generated (in the same way as in the *Close* move), $\mathbf{r}_1, \ldots, \mathbf{r}_{\bar{M}-1}$ for the beads $prev^1(\alpha)$, $prev^2(\alpha)$, ..., $prev^{(\bar{M}-1)}(\alpha)$, respectively. One may now rename $\mathcal{I}$ into ζ, and vice versa, and re-link beads in the following manner: former $prev^{(\bar{M}+1)}(\alpha)$ becomes $prev(\mathcal{I})$, etc. As a result of this world-line reconnection, a piece of world line between the original bead ζ and the bead α is erased, while a new piece of world line appears that connects the former bead $\mathcal{I}$ with the bead α. The move is accepted with probability

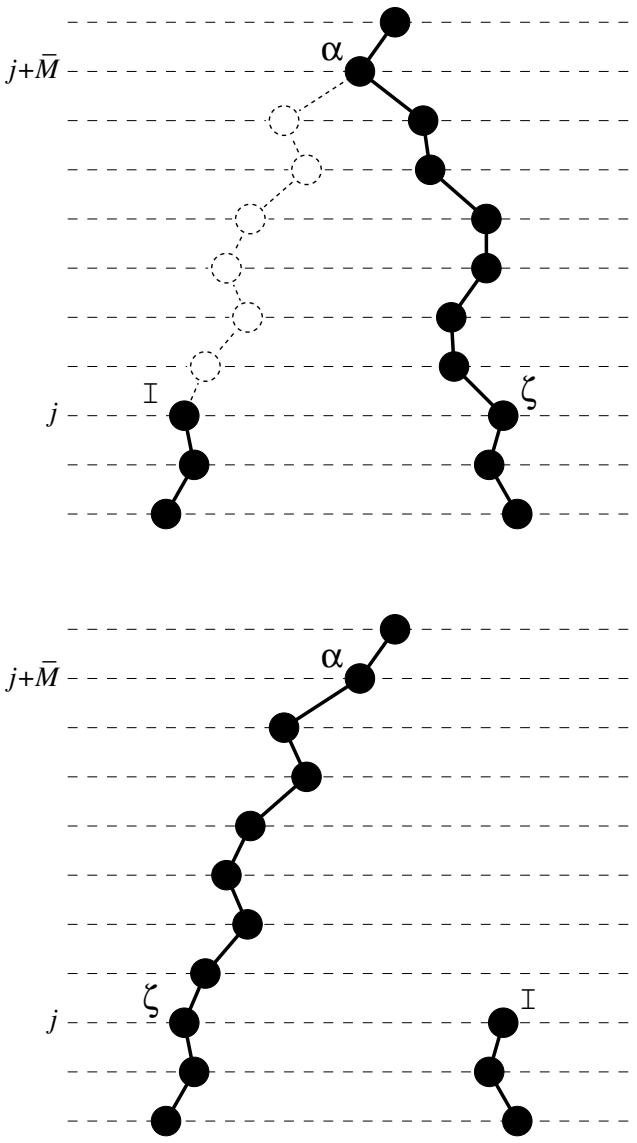

FIG. 2: An illustration of the *Swap* update and the notation introduced in the main text.

$$P_{\rm sw} \;=\; \min\{1,\, {\rm e}^{\Delta U}\Sigma_{\mathcal{I}}/\Sigma_\zeta\} \;. \tag{2.24}$$

Here Σ_ζ is defined similarly to $\Sigma_{\mathcal{I}}$ in Eq. (2.23) using the $\mathcal{L}_\zeta$-list.

The *Swap* move generates all possible many-body permutations through a chain of local single-particle updates. Since no two particles need be brought within

a distance of the order of the hard core of a typical interatomic potential potential, this move enjoys a high acceptance rate, similar to that for the *Advance/Recede* updates (we provide a quantitative example of acceptance ratios measured in simulations of the two-dimensional ^{4}He liquid below). It must be emphasized that in our algorithm, unlike in conventional PIMC, arbitrary permutations of identical particles, as well as macroscopic exchange cycles need not be explicitly sampled. For, they *appear automatically*, if the physical conditions warrant them. This is because the statistics of the relative positions for the worm ends is given exactly by the Green function $G(\mathbf{r}_1, \mathbf{r}_2, \tau)$.

In a typical *sweep*, a worm is created (either by opening an existing closed world line, or by inserting a new one), advances and/or recedes in imaginary time and performs a number of swaps, until it finally closes or is removed. It is easy to convince oneself that, as a result of this procedure, an exchange cycle involving a macroscopic number of particles can appear in just one sweep.

Since the complementary pairs are detail-balanced, the final results do not depend on the global probability of addressing each pair, so long as the probabilities of addressing each update within a complementary pair are *equal*, which is assumed in the acceptance probabilities presented above. Otherwise, the acceptance probabilities should be modified as follows: if the probability to address update A is u_A and the probability to address a complementary update is u_B then $P_A \to P_A(u_B/u_A)$.

As noted in the Introduction, the description of WA given above is complete even without expansion of the pairwise potential tail into diagrams (described below). In the original version of the code we did not use this efficiency enhancing modification of the conventional PIMC configuration space, and still were able to perform accurate studies of several hundred atoms. Since expansion into diagrams works only for the attractive part of the potential it can not be used for purely repulsive models.

III. PHYSICAL ESTIMATORS

The statistical estimators for all physical quantities that are computed in the Z-sector, including those of all energetic and structural properties, are identical with those utilized in conventional PIMC. We therefore refer the reader to Ref. 2 for a detailed discussion of these estimators. Instead, we focus our discussion here on the estimator that is a characteristic feature of the WA, namely that of the Matsubara Green function.

A. Green function and density matrix estimators

Since the Green function is sensitive only to relative distances in time, without loss of generality we can fix $j_{\mathcal{M}} = 0$ to simplify the notation. For an extra simplicity, we will also assume that at least one of the following two statements is true: (i) The problem is translationally invariant in the coordinate space. (ii) The quantity of interest is the Green function averaged over spatial translations,

$$\bar{G}(\mathbf{r}, \tau) \;=\; V^{-1} \int d\mathbf{r}'\, G(\mathbf{r}+\mathbf{r}', \mathbf{r}', \tau)\;. \qquad (3.1)$$

In both cases we can formally fix $\mathbf{r}_{\mathcal{M}} = 0$. [The generalization of the treatment to the case of two independent spatial coordinates is straightforward.]

Consider the configurations, or path-integral diagrams, $\mathcal{D}_\xi(\mathbf{r}_{\mathcal{I}}, j_{\mathcal{I}})$ contributing to the function $g(\mathbf{r}, \varepsilon j)$:

$$g(\mathbf{r}_{\mathcal{I}}, j_{\mathcal{I}}) \;=\; \sum_\xi \mathcal{D}_\xi(\mathbf{r}_{\mathcal{I}}, j_{\mathcal{I}})\;. \qquad (3.2)$$

The subscript ξ stands for all variables of the diagram except for the end point space-time positions. That is ξ contains both positions of the beads (in which case the summation is understood as integration) and a topological structure of the world lines on the β-cylinder.

Comparing the diagrams with different $j_{\mathcal{I}}$ and $\mathbf{r}_{\mathcal{I}}$ (incidentally, it is precisely this comparison that stands behind the acceptance probabilities of *Advance* update), we readily see that given some diagram $\mathcal{D}_{\xi_0}(\mathbf{r}_0, j_0)$ we can "upgrade" it to a diagram $\mathcal{D}_\xi(\mathbf{r}, j)$ with $j > j_0$ by attaching to $\mathcal{I}$ a world line piece of $M = j - j_0$ beads. Specifically,

$$\mathcal{D}_\xi(\mathbf{r}, j) = \mathcal{D}_{\xi_0}(\mathbf{r}_0, j_0)\, R_{j_0 j}(\mathbf{r}_0, \mathbf{r}) \qquad (j_0 < j)\;, \qquad (3.3)$$

$$R_{j_0 j}(\mathbf{r}_0, \mathbf{r}) = \mathrm{e}^{\Delta U + \mu\varepsilon M} \prod_{\nu=1}^{M} \rho_\circ(\mathbf{r}_{\nu-1}, \mathbf{r}_\nu, \varepsilon)\;, \qquad (3.4)$$

where $\xi = \{\xi_0, \mathbf{r}_1, \mathbf{r}_2, \ldots, \mathbf{r}_{M-1}\}$, $\mathbf{r}_M \equiv \mathbf{r}$, and the meaning of ΔU is the same as in *Advance* update: $\Delta U = U_{\xi_0} - U_\xi$, where U_ξ and U_{ξ_0} correspond to the diagrams D_ξ and D_{ξ_0}, respectively. Hence, we have

$$g(\mathbf{r}, \varepsilon j) = \sum_{\xi_0} \int d\mathbf{r}_0 \ldots d\mathbf{r}_{M-1}\, \mathcal{D}_{\xi_0}(\mathbf{r}_0, j_0)\, R_{j_0 j}(\mathbf{r}_0, \mathbf{r}) =$$

$$\frac{1}{\bar{M}} \sum_{\xi_0, j_0} \int d\mathbf{r}_0 \ldots d\mathbf{r}_{M-1}\, \mathcal{D}_{\xi_0}(\mathbf{r}_0, j_0)\, R_{j_0 j}(\mathbf{r}_0, \mathbf{r}) \delta^{(\bar{M})}_{j_0 j}, \quad (3.5)$$

where

$$\delta^{(\bar{M})}_{j_0 j} \;=\; \begin{cases} 1\;, & \text{if } \; j_0 \in [j - \bar{M}, j-1]\;, \\ 0\;, & \text{otherwise}\;. \end{cases} \qquad (3.6)$$

Though Eq. (3.6) is not the final answer yet, it already contains an important element. It allows one to sample the time slice j from the adjacent time slices $j_0 \in [j - \bar{M}, j-1]$. The problem with Eq. (3.6) is that we still have a continuous variable $\mathbf{r}$ while we would like to know the Green function only at the discrete set of pre-defined points $\{\mathbf{r}_p\}$. To proceed further, we utilize

(and to a certain extent generalize) the idea which has been already used in diagrammatic Monte Carlo.[22] Suppose we are interested in $g(\mathbf{r}_p, \varepsilon j)$, where $\mathbf{r}_p \in V_p$ is a pre-selected point for collecting statistics and V_p is a 3D volume containing this point. We formally rewrite (3.5) at point $\mathbf{r}_p$ as (below $\mathbf{r}_M \equiv \mathbf{r}_p$)

$$g(\mathbf{r}_p, \varepsilon j) = \sum_{\xi_0, j_0} \int d\mathbf{r}_0 \, \mathcal{D}_{\xi_0}(\mathbf{r}_0, j_0) \, \delta^{(\bar{M})}_{j_0 j} \times \int d\mathbf{r} \, W_M(\mathbf{r}_0, \mathbf{r}) \, \delta^{(V_p)}_{\mathbf{r}} \times \int d\mathbf{r}_1 \ldots d\mathbf{r}_{M-1} \, \frac{\prod_{\nu=1}^{M} \rho_\circ(\mathbf{r}_{\nu-1}, \mathbf{r}_\nu, \varepsilon)}{\rho_\circ(\mathbf{r}_0, \mathbf{r}_p, \varepsilon M)} \, Q \, , \tag{3.7}$$

$$Q \;=\; (\bar{M} V_p)^{-1} \, \frac{\rho_\circ(\mathbf{r}_0, \mathbf{r}_p, \varepsilon M)}{W_M(\mathbf{r}_0, \mathbf{r})} \, \mathrm{e}^{\Delta U + \mu \varepsilon M} \;\; , \tag{3.8}$$

$$\delta^{(V_p)}_{\mathbf{r}} \;=\; \begin{cases} 1 \, , & \text{if } \; \mathbf{r} \in V_p \, , \\ 0 \, , & \text{otherwise} \, . \end{cases} \tag{3.9}$$

The value of ΔU corresponds to the extra piece of world line $(\mathbf{r}_0, \mathbf{r}_1, \ldots, \mathbf{r}_{M-1}, \mathbf{r}_p)$. In principle, $W_M(\mathbf{r}_0, \mathbf{r})$ is an arbitrary function, but we want it to be positive-definite and normalized (the integration is over the whole system volume, not just V_p), i.e. to have the meaning of the probability density

$$\int d\mathbf{r} \, W_M(\mathbf{r}_0, \mathbf{r}) \;=\; 1 \, . \tag{3.10}$$

Moreover, for our purposes the most reasonable choice is simply

$$W_M(\mathbf{r}_0, \mathbf{r}) \;=\; \rho_\circ(\mathbf{r}_0, \mathbf{r}, \varepsilon M) \, . \tag{3.11}$$

Now we just need to interpret the relation (3.7) in terms of a stochastic process. First, we integrate/sum this relation over the position of $\mathcal{M}$ in space/time and compensate for that by dividing (3.7) by PV. To interpret the first line in (3.7), we recall that in accordance with (2.7) the value of $\mathcal{D}_{\xi_0}$ is equal to the probability density to sample the corresponding diagram of the G-sector times the factor Z_W/C. Hence, we can interpret the first line as averaging—over the ensemble of *all* Monte Carlo diagrams—of the *stochastic variable* given by the rest of the expression times projector $\delta^{(G)}$ times projector $\delta^{(\bar{M})}_{(j_\mathcal{I} - j_\mathcal{M}), j}$ times Z_W/CVP. The second line says that the evaluation of the stochastic variable starts with sampling a vector $\mathbf{r}$ distributed in accordance with Eq. (3.11). The projector $\delta^{(V_p)}_{\mathbf{r}}$ means that if $\mathbf{r} \notin V_p$, then the stochastic variable is automatically zero. If $\mathbf{r} \in V_p$, then the evaluation procedure continues in accordance with the third line of Eq. (3.7), which we interpret as sampling $(M-1)$ auxiliary variables, $\mathbf{r}_1, \ldots, \mathbf{r}_{M-1}$, where $M = j - j_\mathcal{I} + j_\mathcal{M}$. (In the special case of $M = 1$, auxiliary variables are not sampled.) The auxiliary variables are sampled from the distribution

$$\frac{\rho_\circ(\mathbf{r}_0, \mathbf{r}_1, \varepsilon) \rho_\circ(\mathbf{r}_1, \mathbf{r}_2, \varepsilon) \ldots \rho_\circ(\mathbf{r}_{M-1}, \mathbf{r}_p, \varepsilon)}{\rho_\circ(\mathbf{r}_0, \mathbf{r}_p, \varepsilon M)} \, . \tag{3.12}$$

When these are fixed, the stochastic variable in question—up to the global pre-factors discussed above—is nothing other than Q, defined by Eq. (3.8).

Summarizing, we have derived the estimator

$$\langle \, \delta^{(G)} \, \delta^{(\bar{M})}_{(j_\mathcal{I} - j_\mathcal{M}), j} \, \delta^{(V_p)}_{\mathbf{r}} \, Q \, \rangle_{\mathrm{MC}} \;=\; \frac{CVP}{Z_W} \, g(\mathbf{r}_p, \varepsilon j) \, , \tag{3.13}$$

where the variable Q is calculated in accordance with Eq. (3.8) in terms of the auxiliary variables of the above-described procedure, which we illustrate in Fig. 3,

$$Q \;=\; \frac{1}{\bar{M} V_p} \, \frac{\rho_\circ(\mathbf{r}_0, \mathbf{r}_p, \varepsilon M)}{\rho_\circ(\mathbf{r}_0, \mathbf{r}, \varepsilon M)} \, \mathrm{e}^{\Delta U + \mu \varepsilon M} \, .$$

The free parameters of the procedure, $\bar{M}$ and V_p, are optimized to yield the best possible convergence.

Our final note is that if one is interested in the Green function at a certain momentum $\mathbf{p}$ then the corresponding estimator does *not* require any elaboration presented above due to extra integration over $\mathbf{r}$. Indeed, according to Eq. (2.13) we have

$$\langle \, \delta^{(G)} \, \delta_{j, (j_\mathcal{I} - j_\mathcal{M})} \, e^{i\mathbf{p}(\mathbf{r}_\mathcal{I} - \mathbf{r}_\mathcal{M})} \, \rangle_{\mathrm{MC}} \;=\; \frac{CVP}{Z_W} \, g(\mathbf{p}, \varepsilon j) \, . \tag{3.14}$$

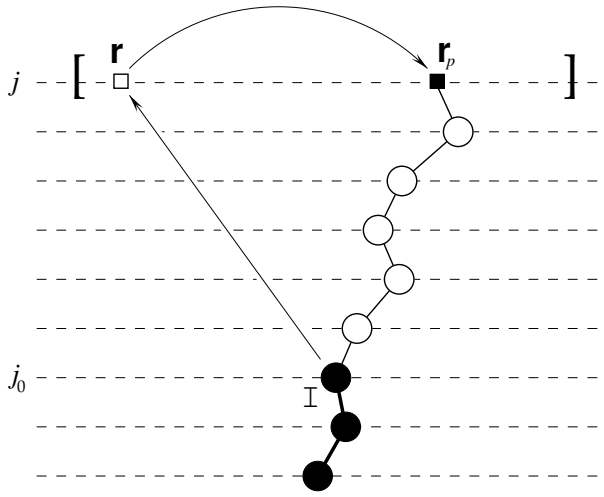

FIG. 3: Construction of the estimator for the Green function $G(\mathbf{r}_p, \varepsilon j)$, where without loss of generality we assume that $\mathbf{r}_\mathcal{M} = 0$, $j_\mathcal{M} = 0$.

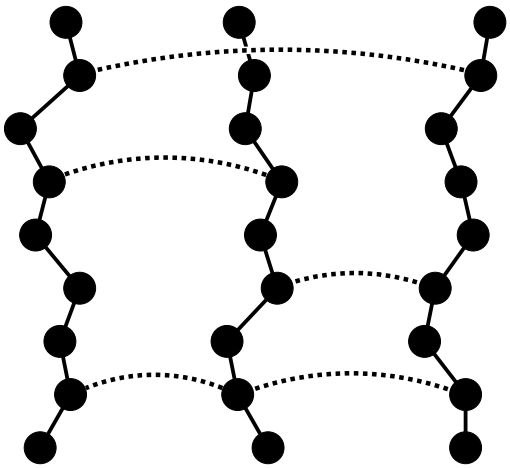

FIG. 4: Configuration space with diagrammatic bonds between the equal-time beads.

IV. ENHANCED VERSION: DIAGRAMMATIC EXPANSION OF THE ATTRACTIVE POTENTIAL TAIL

The WA described in II can be (and, has been) used for efficient simulations of systems comprising a few hundred particles. This section describes a general procedure that significantly improves performance of PIMC, through an efficient sampling of the contribution of the attractive tail of the pair potential. The trick *per se* is not directly related to the WA, and can be implemented within other PIMC schemes. Obviously, the modification of the configurational space it brings about should be adequately taken into account in the updates. Moreover, in order for the trick to be applicable an attractive tail of the interparticle potential must exist, i.e., what described below does not apply to purely repulsive interactions, such as hard-sphere.

Straightforward schemes for calculating the potential energy exponent of a multi-particle path, $U(X)$, have to deal with a compromise between accuracy and performance. By a "straightforward scheme", we mean one that treats the pair interaction between *any* two particles on the same footing, irrespectively of the value of the potential, as long as it is non-zero, which is the case in all realistic models. The computational complexity of such schemes scales linearly with N per single-particle update. To improve on efficiency, one typically truncates the potential at some distance, thus introducing a systematic error.

There is, however, a way to reduce radically the computational effort required for accurate treatment of the potential tail, *without* introducing any additional systematic error. The only price to pay is a more complex configuration space (see Fig. 4) and, correspondingly, additional updates to sample it.

We confine ourselves to the simplest case, i.e., the one in which $U(X)$ is a sum of pairwise contributions:

$$U \;=\; \sum_{j=0}^{P-1} \sum_{\langle a_j b_j \rangle} u(\mathbf{r}_{a_j} - \mathbf{r}_{b_j}) \;, \tag{4.1}$$

where beads on the j-th time slice are labeled using subscripts a_j and b_j, the notation $\langle a_j b_j \rangle$ stands for all pairs of beads on a given slice, and $\mathbf{r}$'s are the spatial coordinates of the beads. In the simplest[2] choice for U $u(r) = v(r)\varepsilon$. Correspondingly,

$$\mathrm{e}^{-U} \;=\; \prod_{j} \prod_{\langle a_j b_j \rangle} \mathrm{e}^{-u(\mathbf{r}_{a_j} - \mathbf{r}_{b_j})} \;. \tag{4.2}$$

An important observation now is that if $|\mathbf{r}_{a_j} - \mathbf{r}_{b_j}| > r_c$, where r_c is some distance, greater than the radius of the repulsive core of the pair potential, then $u(\mathbf{r}_{a_j} - \mathbf{r}_{b_j}) < 0$, and the corresponding pairwise exponential can be identically split into a sum of two positive definite terms:

$$\mathrm{e}^{-u(\mathbf{r}_{a_j} - \mathbf{r}_{b_j})} \;=\; 1 + \left[\mathrm{e}^{-u(\mathbf{r}_{a_j} - \mathbf{r}_{b_j})} - 1 \right] \;. \tag{4.3}$$

Graphically, this decomposition can be represented as follows: Any two beads within one and the same slice with $|\mathbf{r}_{a_j} - \mathbf{r}_{b_j}| > r_c$, now may or not share an extra graphical element, a *bond*, see Fig. 4. The new configuration space is reminiscent of the Feynman's diagrammatic expansion in powers of the interaction potential. The absence of a bond between two beads a_j and b_j represents the first term in Eq. (4.3), i.e. unity, and means that the beads at a distance $|\mathbf{r}_{a_j} - \mathbf{r}_{b_j}| > r_c$ do *not* interact. A bond between beads a_j and b_j represents the second term of Eq. (4.3). Its relative contribution to the statistics as compared to the case of no bond has an extra factor of

$$\mathrm{e}^{-u(\mathbf{r}_{a_j} - \mathbf{r}_{b_j})} - 1 \qquad \text{(bond factor)} \;. \tag{4.4}$$

If one of the beads in the bond is a worm, then the bond factor is

$$\mathrm{e}^{-u(\mathbf{r}_{a_j} - \mathbf{r}_{b_j})/2} - 1 \qquad \text{(worm bond factor)} \;. \tag{4.5}$$

Formally, we attribute potential energy exponents to beads, but in reality they represent interactions between the world line trajectories; since the worm bead has a trajectory attached to it from one side only, its potential energy exponent is reduced by a factor of two. Correspondingly, the two worm beads do not interact and thus $\mathcal{I}$ can not be connected by the bond to $\mathcal{M}$.

The standard MC prescription for sampling the new configuration space would be to have updates which create and remove bonds. It is easy to see how a "radical gain in performance" can be achieved, as, statistically, the probability for two beads a_j and b_j with $|\mathbf{r}_{a_j} - \mathbf{r}_{b_j}| > r_c$ to share a bond is much smaller than unity. Indeed, this probability is proportional to the bond factor

(4.4), which can be estimated as $\sim v(r)\varepsilon \ll 1$. In order to sample the new configuration space, we introduce a pair of complementary updates that create and remove bonds. This pair of updates is reminiscent of diagrammatic Monte Carlo updates that create and delete beads. There is, however, an important mathematical difference. When creating new beads one has to seed new continuous variables associated with them. Bonds are created between existing beads, and formally the new updates are of the standard Metropolis type.

Create Bond. The update is only possible if the configuration is off-diagonal. An integer number M is selected at random within the interval $[0, \bar{M}]$; $\bar{M} < P$. This number is used to select the first bead, $a_j \equiv prev^M(\mathcal{I})$, in the pair to be connected by the bond. If $prev^M(\mathcal{I})$ is not defined because the world line terminates at $\mathcal{M}$, the update is rejected. The second bead, b_j, is selected in two steps. First, within the slice j of the bead a_j we select a spatial bin, $\mathcal{B}$. This is done by randomly generating the bin label from some probability distribution, $P_{\mathcal{AB}}$, which, in general, depends on the distance between $\mathcal{B}$ and the bin A that contains the first bead a_j. (We discuss a reasonable choice of $P_{\mathcal{AB}}$ below.) Let $n_{\mathcal{B}}$ be the number of beads in the bin $\mathcal{B}$. If $n_{\mathcal{B}} = 0$, the update is rejected. If $n_{\mathcal{B}} > 0$, we select at random a bead from the bin $\mathcal{B}$ and call it b_j. If it happens that $a_j = \mathcal{I}$ and $b_j = \mathcal{M}$ the update is rejected because physically the world line ends do not interact. Also, if a_j and b_j are already connected by a bond, or the distance between the selected beads is smaller than r_c, the update is rejected. Otherwise, we propose to create a bond between the selected pair of beads, and accept the proposal with the probability

$$P_{\rm crb} \;=\; \frac{(\bar{M}+1)n_{\mathcal{B}}}{(l_{\rm bnd}+1)P_{\mathcal{AB}}}\,\left[\,{\rm e}^{-f u(\mathbf{r}_{a_j}-\mathbf{r}_{b_j})}-1\,\right]\,. \qquad (4.6)$$

Here $l_{\rm bnd}$ is the *total* number of bonds in the initial configuration associated with the beads $\mathcal{I}$, $prev(\mathcal{I})$, ..., $prev^{\bar{M}}(\mathcal{I})$ or $\mathcal{I}$, $prev(\mathcal{I})$, ..., $\mathcal{M}$ if $prev^{\bar{M}}(\mathcal{I})$ is not defined. The balancing factor $(l_{\rm bnd}+1)$ naturally emerges from the *Remove Bond* update which is complementary to the *Create Bond*. An additional factor $f = 1/2$ in the exponent is necessary only if one of the beads in the pair is the world line end; otherwise, $f = 1$.

Remove Bond. The update is only possible if the configuration is off-diagonal. We list all $l_{\rm bnd}$ bonds associated with the beads $\mathcal{I}$, $prev(\mathcal{I})$, ..., $prev^{\bar{M}}(\mathcal{I})$ or $\mathcal{I}$, $prev(\mathcal{I})$, ..., $\mathcal{M}$ if $prev^{\bar{M}}(\mathcal{I})$ is not defined. If $l_{\rm bnd} = 0$, the update is rejected. Otherwise, we randomly select a bond from the list and propose to remove it. The acceptance probability for the update is

$$P_{\rm rmb} \;=\; \frac{l_{\rm bnd}P_{\mathcal{AB}}}{(\bar{M}+1)n_{\mathcal{B}}}\,\left[\,{\rm e}^{-f u(\mathbf{r}_{a_j}-\mathbf{r}_{b_j})}-1\,\right]^{-1}\,. \qquad (4.7)$$

From Eqs. (4.6)-(4.7) we realize that an optimal choice for $P_{\mathcal{AB}}$ is based on the interaction potential between the bin centers

$$P_{\mathcal{AB}} \;\propto\; {\rm e}^{-u(\vec{\mathcal{R}}_{\mathcal{B}}-\vec{\mathcal{R}}_A)}-1 \;\approx\; -u(\vec{\mathcal{R}}_{\mathcal{B}}-\vec{\mathcal{R}}_A)\,. \qquad (4.8)$$

An estimator for the bond contribution to the potential energy, $U_{\rm bonds}$, is obtained using a standard trick of replacing $v(r) \to \lambda v(r)$ and then utilizing the identity

$$\langle\, U\,\rangle \;=\; -\frac{1}{\beta Z}\,\frac{dZ}{d\lambda}\,\Big|_{\lambda=1}\,, \qquad (4.9)$$

in accordance to which each Z-configuration is differentiated with respect to λ, and then λ is set to unity. The contribution to the derivative from the bond factors (4.4) yields

$$U_{\rm bonds} \;=\; \frac{1}{\beta}\,\frac{\langle\,\delta^{(Z)}\sum_b u_b/(1-e^{u_b})\,\rangle_{\rm MC}}{\langle\,\delta^{(Z)}\rangle_{\rm MC}}\,, \qquad (4.10)$$

where the sum is over all bonds in a current configuration.

A. Worm updates within the diagrammatic bonds

How does the presence of bonds affect the worm updates? The answer depends on the updating scenario. The easiest way is to work with the same updating procedures we had without bonds. The only extra price is then in having simple constraints on the updates applicability to a given configuration. Namely, we require that all the beads being either deleted, or created, or shifted as a result of worm updates be free of bonds. Special care of bond factors has to be taken when interconverting regular beads to worms [see Eqs. (4.4) and (4.5)].

The above requirement is not, in practice, as restrictive as one might think, since the probability of having no bonds at $\bar{M}$ consecutive beads is of order unity, with the proper choice of parameters discussed in the next Section.

A brief qualitative discussion of the parameter r_c is in order here. Formally, r_c can be as small as the size of the repulsive core of the potential, to guarantee the positive definiteness of the second term in Eq. (4.3). It turns out, however, that this choice is not optimal, because in this case the total number of bonds per $\bar{M}$ consecutive beads of a world line may grow large (assuming that $\bar{M}$ is optimized in terms of the worm updates), and the above-mentioned condition of absence of bonds, in order for worm updates to be performed, may be satisfied very infrequently; consequently, the scheme may become inefficient. In the next Section we show that for helium, r_c is slightly larger than the radius of the first coordination shell. For best performance, both $\bar{M}$ and r_c should be simultaneously optimized.

Finally, we note that it is possible to generalize the diagrammatic procedure to cases when the $e^{-U(X)}$ exponential does not factor into pairwise terms. A great simplification here comes from the observation that for any particular choice of $U(X)$, factorization does take place at least to the first approximation. The correcting terms are then of the form of close-to-unity three-bead, four-bead (and so forth) factors. The larger the number of beads in the correcting factor, the closer the correcting factor is to unity in terms of the powers of ε. This

observation immediately suggests a recurrent (perturbative) scheme, which consists of ascribing correction factors to the diagrams, depending on the number of beads in the bond-connected cluster. The description of such a scheme goes beyond the scope of the present paper, since we find that higher-order corrections can be safely neglected for the realistic choice of r_c discussed in the next Section.

V. ADDITIONAL NOTES ON THE OPTIMAL ALGORITHM PARAMETERS FOR ^{4}HE.

The separation radius for the diagrammatic expansion is determined from two conditions which ensure high performance of the algorithm. For efficient *Swap* updates one has to keep the length (in imaginary time) of the updated trajectory long enough to avoid proposing large displacements over short time periods. If a_0 is the interatomic distance, then the parameter $\bar{M}$ must satisfy the condition

$$\bar{M} \sim \frac{(a_0/2)^2 m}{2\varepsilon} \,, \tag{5.1}$$

which for ^{4}He with $a_0 = 3.5$ Å gives $\bar{M} \sim 25$ assuming relatively small $\varepsilon = 5 \times 10^{-3}\, K^{-1}$.

Since *Swap* and other updates are performed on trajectory pieces having no bonds on the corresponding time intervals, it is important to have also

$$\langle\, l_{\rm bnd}(\bar{M})\,\rangle \;\sim\; 1 \,, \tag{5.2}$$

where $\langle l_{\rm bnd}(\bar{M})\rangle$ is the average number of bonds on the trajectory interval of length $\bar{M}\varepsilon$. If this number is large, the simple updating strategy presented above will become inefficient due to small probability of fluctuations to the state with $l_{\rm bnd}(\bar{M}) = 0$. In practice, the computational cost of calculating acceptance ratios in the strongly-correlated system is much larger than a simple check for the presence of bonds; thus, the above condition can be easily extended to $\langle l_{\rm bnd}(\bar{M})\rangle \approx 2$.

The number of bonds per time interval can be readily estimated from the pairwise interaction potential by using a mean-field estimate for the chemical potential shift

$$\langle l_{\rm bnd}\rangle \;\approx\; \bar{M}\varepsilon n \int_{r_c}^{\infty} d^d r\; v(r)\; g(r) \;\approx\; \bar{M}\varepsilon n \int_{r_c}^{\infty} d^d r\; v(r) \,, \tag{5.3}$$

where $g(r)$ is the pair correlation function, which tends to 1 in the $\mathbf{r} \to \infty$ limit. The last approximation in Eq. (5.3) is quite accurate for r greater than a few times a_0. For the Aziz pair potential, $\bar{M}\varepsilon = 0.125\, K^{-1}$, and particle number density $n = 0.025$ Å^{-3} we have the condition $\langle l_{\rm bnd}\rangle \approx 2$ satisfied for

$$r_c \approx 4.2 \text{ Å} \,, \tag{5.4}$$

in three dimensions. This radius falls in between the first and second peaks of the pair correlation function, and, roughly speaking, includes the first coordination sphere of ^{4}He atoms. Thus, on average, not more than 12 neighboring particles are contributing to the potential energy term in the exponent for the configuration weight of the trajectory. It should be stressed that the above set of control parameters is, of course, merely an approximate guideline. To give a concrete example, for simulations of liquid helium near the λ-point at the saturated vapor pressure (SVP), we find that $r_c = 4$ Å and $\bar{M}\varepsilon \approx 0.125$ is a reasonable choice.

The advantage of using sophisticated forms of $U(X)$, lies in the fact that one may achieve the same accuracy in evaluating the configuration weight, with smaller number of time slices (see Ref. 2 for an exhaustive discussion of this aspect). Below we discuss the scheme suggested in Ref. 23, which takes into account the first derivatives of the interparticle potential (this is the scheme that we have adopted in all calculations presented below):

$$U(X) = \sum_{j=2k} \frac{2\varepsilon}{3}\, v(\mathbf{R_j}) + \sum_{j=2k+1} \left[\frac{4\varepsilon}{3}\, v(\mathbf{R_j}) + \frac{\varepsilon^3}{9m}\, F(\mathbf{R_j}) \right] , \tag{5.5}$$

where

$$F(\mathbf{R_j}) = \sum_{i=1}^{N} \mathbf{f}_i^2 \equiv \sum_{i=1}^{N} \left(\sum_{j\neq i}^{N} \mathbf{f}_{ij} \right)^2 \equiv \sum_{i=1}^{N} \left(\sum_{j\neq i}^{N} \frac{\partial v}{\partial \mathbf{r}_{ij}} \right)^2 , \tag{5.6}$$

sums squares of forces acting on particles. The "force" term is very important in the repulsive region of the potential and close to the point where $v(r)$ changes sign. In this region $v(r)$ derivatives are large and their contribution to the configuration weight may become comparable to the leading linear in ε terms on some slices.

Let us separate in Eq. (5.6) contributions coming from forces between close ($r_{ij} < r_c$) and distant ($r_{ij'} > r_c$) pairs (we label them with indexes 1 and 2 respectively), $F = F_1 + F_2 + F_{12}$:

$$\begin{aligned} F_1 \;&=\; \sum_{i=1}^{N} \left(\sum_{j\neq i} \mathbf{f}_{ij}^{(1)} \right)^2 ; \quad F_2 = \sum_{i=1}^{N} \left(\sum_{j'\neq i} \mathbf{f}_{ij'}^{(2)} \right)^2 ; \\ F_{12} \;&=\; 2 \sum_{i=1}^{N} \left(\sum_{j\neq i} \mathbf{f}_{ij}^{(1)} \right) \cdot \left(\sum_{j'\neq i} \mathbf{f}_{ij'}^{(2)} \right) . \end{aligned} \tag{5.7}$$

If only F_1 and F_{12} terms were present, the diagrammatic expansion would be easy to modify to include these terms into the consideration. The F_1 term is accounted for directly in the weight exponent by keeping records of short-range forces acting on particles and updating them accordingly. We assume that this procedure is always implemented and discuss below only how to deal with the force term in the diagrammatic expansion of the potential tail.

The F_{12} term modifies the diagram weight and acceptance ratios for the diagrammatic updates. Now, the relative weight of configurations with and without a bond between distant (odd) beads a and b is given by the same

formula (4.4) with

$$u_{ab} = \frac{4\varepsilon}{3} v(r_{ab}) + \frac{2\varepsilon^3}{9m} (\mathbf{f}_a^{(1)} - \mathbf{f}_b^{(1)}) \cdot \mathbf{f}_{ab}^{(2)} \ . \qquad (5.8)$$

Since the procedure of keeping track of forces acting on particles is standard for high-accuracy PIMC schemes, the required modifications of the scheme are minimal. [Note that short-range forces are present now in the expression for the bond factor (5.8), and thus their possible effects on bonds should be accounted for whenever these forces change].

Dealing with the F_2 term is more cumbersome. Its exact treatment requires a solution of recursive relations for every chain of beads connected by the diagrammatic expansion. At this point we notice that forces between distant particles are *orders of magnitude* smaller than forces acting at short distances $r < 2.6$ Å and thus can be safely neglected. Indeed, for $r_c = 4.5$ Å and $\varepsilon = 5 \times 10^{-3}\ K^{-1}$, the F_2 term can be estimated to be of order of 10^{-6} and thus has no measurable effect on the simulation results. After all, the interatomic potential is not even known with this accuracy. We conclude then that the diagrammatic expansion can be straightforwardly implemented for the high-accuracy scheme by omitting the F_2 term in the configuration weight.

Formally, due to extremely rare statistical fluctuations which bring two particles at very close distance and result in large forces $\mathbf{f}^{(1)}$ acting on them, the sign of u_{ab} in Eq. (5.8) may change from positive to negative. This, in turn, will change the sign of the configuration weight if the corresponding bond is accepted. One can hardly classify the possibility of such rare events as a "sign problem" because the average configuration sign will remain close to unity, and will not impair the algorithm efficiency. In practice, for $r_c = 4 - 5$ Å and $\varepsilon < 0.01\ K^{-1}$ the configuration sign simply *never* changes during the entire simulation.

Finally, one may wonder if the inclusion of the F_{12} term really helps to achieve better accuracy with smaller number of slices. If the desired accuracy does not exceed three significant digits and r_c is kept larger than 4 Å then the answer is "No". At this level of accuracy, one may implement the diagrammatic expansion for the potential tail by ignoring the force term in the bond factor altogether, i.e. exactly as described in the previous section. Though we have implemented schemes with and without the F_{12} term, we did not detect any difference in final answers when using algorithm parameters specified above. The F_1 term was still kept in the exponent for more accurate evaluation of the short-range part. Alternatively, one may choose to deal with the short-range part using the pair-product approximation of Ceperley and Pollock,[2] making use of tables for the two-particle density matrix calculated for an interaction potential which is identically zero at distances greater than r_c.

VI. SIMULATION RESULTS

In this Section, we present WA simulation results for bulk liquid ^{4}He in two and three dimensions, with the aim of demonstrating that superfluid properties and off-diagonal correlations can be calculated with the WA for very large system sizes, orders of magnitude larger than accessible to the conventional PIMC technology. We use the standard interatomic (Aziz) potential for helium, in an early form for consistency with other calculations.[24] The reason for our choice of illustrative system, is simply that the simulation of ^{4}He in its condensed phase is a *de facto* test bench for new computational many-body techniques.

As mentioned above, we have utilized the form for $U(X)$ suggested in Ref. 23 for all the calculations for which results are presented here. In both two and three dimensions, we have observed convergence of the kinetic energy estimates (computed with the usual thermodynamic estimator[2]) using a time step ε=1/640 K^{-1}; for all other quantities, four times a value of ε can be used, and the estimates are seeing to coincide, within their statistical uncertainties, with those extrapolated to the $\varepsilon \to 0$ limit.

A. ^{4}He in two dimensions

We start with the two dimensional case and extend the study of the superfluid-normal liquid (SF-N) transition first carried out in Ref. 25, at a density $n = 0.0432$ Å^{-2}; we consider system sizes up to hundred times larger than in the original study.[26] In Fig. 5 we present data for the superfluid fraction $\rho_s(T)$, for systems comprising $N = 25$, 200, and 2500 atoms. Since the SF-N transition in 2D is in the Kosterlitz-Thouless universality class,[27] with strong (logarithmic) finite-size corrections, a reliable extrapolation to the thermodynamic limit requires that simulations be performed for significantly different number of particles. In the vicinity of the transition point, one may then employ the asymptotic (in the limit of large distances) vortex-pair renormalization group (RG) theory to fit the data. In our study, we used the same RG procedure as in Ref.[25], which is based on the notion of the vortex core diameter, d (as a short-range cut-off for RG equations), and vortex energy, E_c, to control vortex density at distance d. Only data in the narrow vicinity of the transition point $0.65\ K \le T \le 0.8\ K$ were used in the fitting procedure. Our estimates for the values of the fitting parameters are $d = 8.8 \pm 0.5$ Å for the vortex core diameter, and E=2.18 ± 0.04 K for the vortex energy, which lead to an estimate for the critical temperature T_c=0.653±0.010 K. The vortex diameter (roughly twice the interatomic distance) turns out to be comparable to the linear system size L for $N = 25$, clearly showing that the use of the asymptotic RG analysis is questionable for such a small system size. This fact also explains why our result for T_c is significantly different from the previous

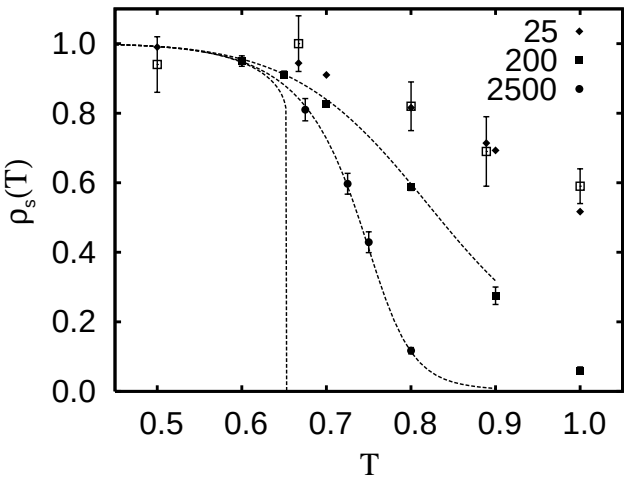

FIG. 5: Superfluid fraction $\rho_s(T)$ computed for 2D ^{4}He on systems with different numbers N of ^{4}He atoms. The system density is $n = 0.0432$ Å^{-2}. Dashed lines represent fits to the numerical data (in the critical region) obtained using the procedure illustrated in Ref.[25]. The leftmost dashed line is the extrapolation to the infinite system. Open squares show results obtained in Ref.[25] for the same system, with N=25.

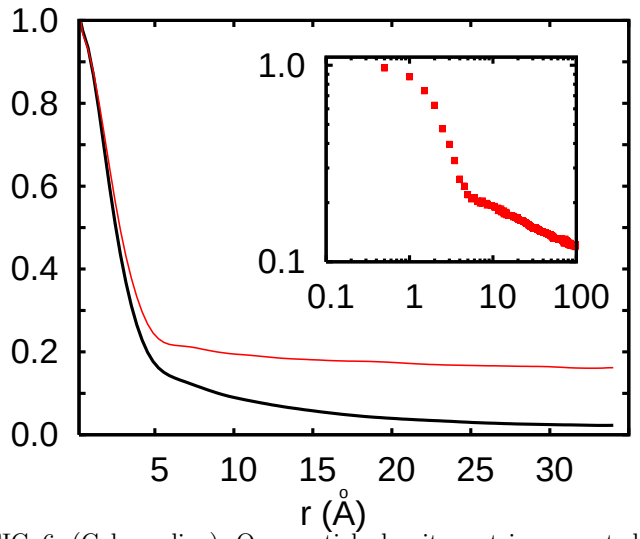

FIG. 6: (Color online). One-particle density matrix computed for 2D ^{4}He at a density $n = 0.0432$ Å^{-2} for a system of 200 atoms, at T=0.675 K (upper curve) and T=1.0 K (lower curve). Statistical errors on the curves are very small, and not shown for clarity. In the inset, we present data (on a log-log scale) for the N=2500 system at T=0.675 K, with clear signatures of the Kosterlitz-Thouless behavior in the vicinity of the critical point. [Reproduced from Ref. 11.]

estimate, 0.72±0.02 K, deduced from the $N = 25$ data.[25]

In Fig. 6, we show results for the single-particle density matrix $n(r)$. For 2D helium, this quantity is expected to decay to zero at all finite temperatures. In the normal phase, and far from the critical point, the decay is exponential. At the critical point, the decay is described by a slow power-law $n(r) \sim 1/r^{1/4}$. The same law should be

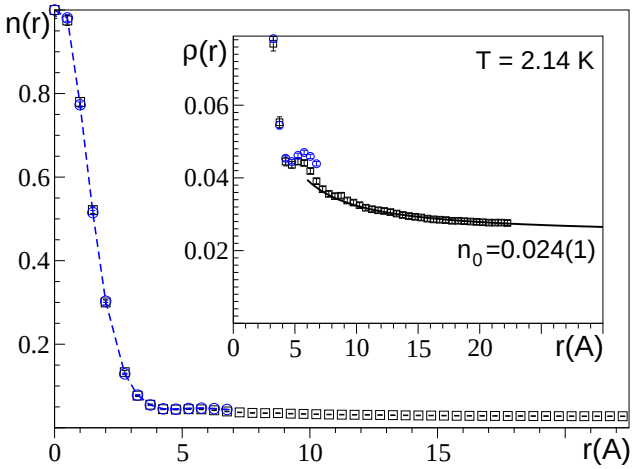

FIG. 7: (Color online). One-particle density matrix $n(r)$ close to the SVP critical point at $T = 2.14$ K for two system sizes $N = 64$ (filled squares) and $N = 2048$ (open squares). The solid line is the theoretical prediction based on long-wavelength phase fluctuations, Eq. (6.1).

observed in the vicinity of the critical point up to exponentially large distances. At low T, the exponent in the power law approaches zero. The data in Fig. 6 are in line with these expectations; quantitatively, the slope of the $n(r)$ curve on the log-log plot shown in the inset is close to one quarter.

We wish to conclude this subsection by giving an example of typical (without any extensive optimization) algorithm parameters used for the two-dimensional helium. For the $T = 1$ K, $\mu = -1$ K, and $N = 25$ system with $P = 200$, $\bar{M} = 40$, $C_0 = 7.5$, and $r_c = 4.05$ Å the measured acceptance probabilities were $P_{\rm op} = 0.47$, $P_{\rm cl} = 0.43$, $P_{\rm in} = 0.13$, $P_{\rm rm} = 0.44$, $P_{\rm ad} = 0.43$, $P_{\rm re} = 0.59$, $P_{\rm sw} = 0.33$, $P_{\rm crb} = 0.58$ $P_{\rm rmb} = 0.42$.

B. ^{4}He in three dimensions

As mentioned in the Introduction, simulations of bulk 3D liquid helium were among the first remarkably successful applications of the PIMC method.[1] However, previous predictions made for the superfluid properties were never at the same level of accuracy as for energetic or structural properties, for reasons mentioned in the Introduction. In this subsection, we show how the WA, based on updates described above, eliminates the shortcomings of the existing PIMC method, by allowing simulations of several thousand atoms with sufficient precision to determine, for example, the critical temperature of the SF-N transition at the saturated vapor pressure (SVP) with accuracy of three significant digits.

In Fig. 7, we show our data for the density matrix $n(r)$ in the vicinity of the critical point, at the saturated vapor pressure (at a temperature T=2.14 K and at a density n=0.02198 Å^{-3}) for system sizes $N = 64$ and $N = 2048$.

Though the data for small and large system sizes appear nearly identical in the main plot, the crucial difference is clearly seen in the inset. The $N = 64$ curve terminates right after the first coordination shell oscillation; the best estimate that can be obtained of the condensate fraction $n_\circ$ (namely, the asymptotic value to which $n(r)$ should plateau at long distances) from this set of data alone, would be about 0.045. Obviously, the same coordination shell oscillation prohibits *a fortiori* any reliable finite-size scaling for smaller system sizes, e.g. using series $N = 16,\ 32,\ 64$.

In contrast, the $N = 2048$ system is large enough to see the effect of long-wavelength hydrodynamic phase fluctuations. The Bogoliubov expression for the asymptotic behavior of $n(r)$ at large distances in the superfluid, is given by

$$n(r) = n_\circ \exp\left[\frac{T}{8\pi\lambda n\rho_s r}\right]. \qquad (6.1)$$

Since ρ_s is calculated independently, the shape of the density matrix decay is fixed. The condensate fraction controls only the overall normalization of the theoretical curve, and this allows precise extrapolation of the data to the thermodynamic limit. An example of such extrapolation is shown in Fig. 7 by the solid line, which predicts $n_0 = 0.024(1)$ for the condensate fraction $n_\circ$ at $T = 2.14\ K$—nearly a factor of two smaller than the 0.045 estimate obtained on a 64-atom system.

The hydrodynamic correction to the tail of $n(r)$ is less important at low temperature and for large values of ρ_s. For comparison, in Fig. 8 we present data for a system of $N = 1024$ atoms, at a temperature $T = 1\ K$ (in this case, the density is n=0.02184 Å^{-3}). In this temperature range, smaller system sizes can be used to obtain reliable thermodynamic estimates of $n_\circ$. Our estimate for $n_\circ$ at T=1 K is 0.082±0.002. This is consistent with the existing PIMC estimate (0.07±0.01 at T=1.2 K, from Ref. 2), obtained on a system of 64 ^{4}He atoms, but somewhat above the most recent T=0 estimate (0.069±0.005, Ref. 28). Although the difference is only slightly greater than the combined statistical uncertainties, it should be noted that finite temperature calculations are *unbiased*, whereas ground state calculations are based on an input trial wave function. While it is in principle possible to remove the variational bias associated to the trial wave function, this may be difficult a goal to achieve in practice.

Having access to system sizes which allow asymptotic hydrodynamic description is a necessary condition for determining critical parameters using finite-size scaling techniques (see, e.g., Ref 29). The idea is to consider quantities which are determined by system properties at the largest scales, becoming scale-invariant at the critical point. For small deviations from criticality, $\delta \to 0$, the dependence on system size for such quantities is given by

$$R(L,\delta) = f_R(L/\xi(\delta)) \equiv g_R(\delta L^{1/\nu}), \qquad (6.2)$$

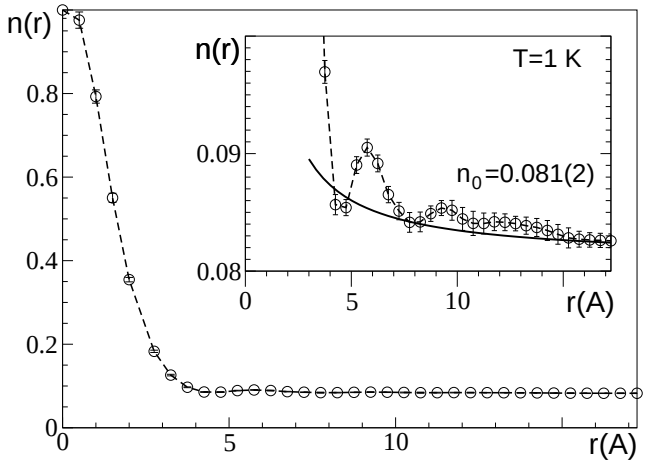

FIG. 8: One-particle density matrix $n(r)$ for $N = 1024$ particles at $T = 1\ K$ and SVP pressure. The solid line is the theoretical prediction based on the long-wave phase fluctuations, Eq. (6.1).

where $f_R(x)$ and $g_R(x)$ are the corresponding universal scaling functions ($g_R(x)$ is analytic at $x = 0$) and $\xi(\delta)$ is the correlation length which diverges at the critical point as $\xi \propto \delta^{-\nu}$. For the U(1) universality class in 3D, the best numerical estimate currently available for the correlation length exponent is $\nu = 0.6717$.[30] The intersection of $R(L,\delta)$ curves for different system sizes provides very accurate and unbiased estimates of critical parameters.

Previous attempts to determine T_c from the scale-invariance of $R(L) = \rho_s L$ (Josephson relation) have failed.[7] Though the authors of Ref. 7 correctly argue that "The statistical uncertainty in the data is too large to accurately determine T_c from the crossing of these [scaling] two curves", it seems that coordination shell oscillations also contribute to several intersections in the 1.6 K $< T <$ 2.4 K interval.

In Fig. 9, we show the temperature dependence of the superfluid fraction for various system sizes. After extrapolation to the thermodynamic limit, there is nearly perfect agreement between the numerical and experimental results. In order to determine the transition temperature T_c, we perform finite-size scaling analysis of

$$R(L,T) = \frac{2\lambda n\rho_s L}{T} = \frac{\langle W^2\rangle}{3},$$

where $\mathbf{W}$=(W_x, W_y, W_z) is the winding number.[5] The raw data are shown in Fig 10. As an independent check, we also draw a horizontal line at the known U(1)-universality class value for winding number fluctuations at the critical point.[30,32] From the intersection of scaling curves (which is seen to take place at the universal value, within the statistical uncertainties), we find $T_c = 2.193(6)$. The difference between this prediction and the experimental value, 2.177 K, is very small, i.e., simulations of the superfluid density dependence on system size in the vicinity of the critical point, do allow us

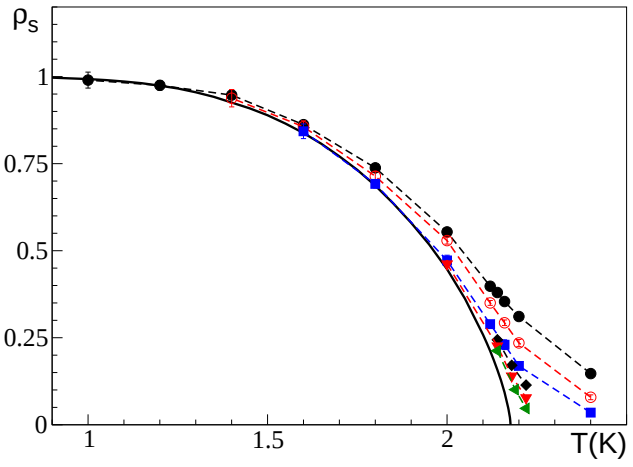

FIG. 9: (Color online). Superfluid fraction $\rho_s(T)$ as a function of temperature at SVP, computed for different system sizes, namely $N = 64$ (filled circles), $N = 128$ (open circles), $N = 256$ (filled squares), $N = 512$ (diamonds), $N = 1024$ (triangles down), and $N = 2048$ (triangles left). The solid line is the experimental curve.

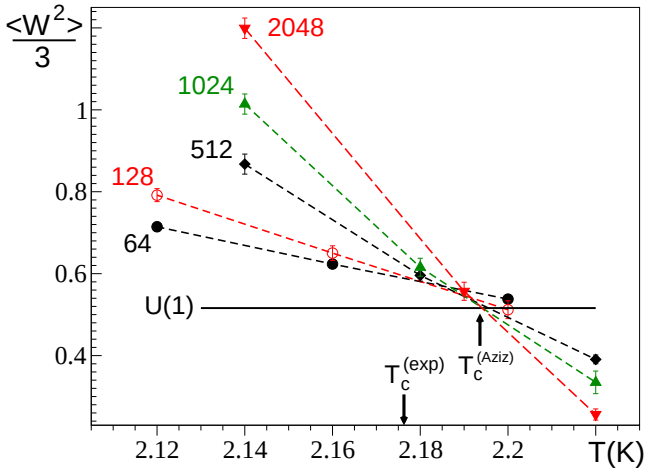

FIG. 10: (Color online). Finite-size scaling plot for $2\lambda n\rho_s L/T = \langle W^2\rangle/3$ at SVP. The solid line is the U(1) universality class value of 0.516(1).

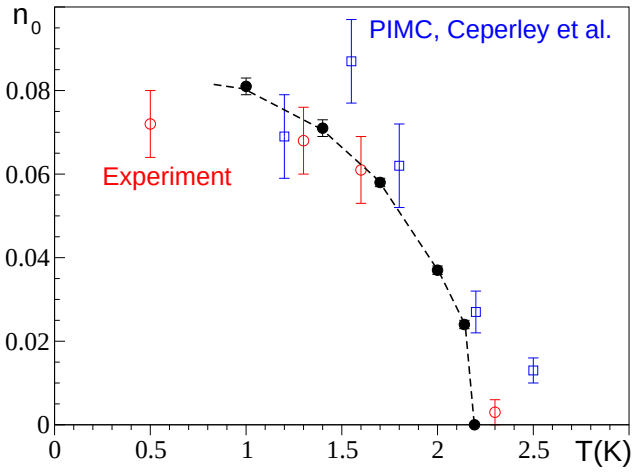

FIG. 11: (Color online). Condensate fraction at the saturated vapor pressure. The dashed line is used to guide the eye.

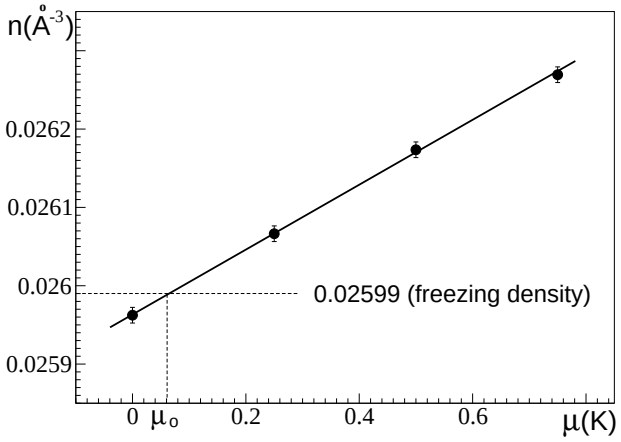

FIG. 12: (Color online). Liquid density as a function of chemical potential at low temperature $T = 0.25$ K. The slope of the solid line is deduced from the simulated values of compressibility averaged over four points shown in the plot. The critical value of the chemical potential deduced from this plot is estimated as $\mu_\circ = 0.06 \pm 0.04$.

to calculate T_c with a relative accuracy of better than 0.5%. There is no reason to expect the Aziz pair potential to reproduce T_c with much better accuracy, as it was not optimized for this purpose. It is only a very good approximation to the true interatomic potential for ^{4}He which, in reality, includes irreducible forces acting between three and more particles.[33]

Condensate density has been consistently one the most difficult properties to compute and measure for helium. Shown in Fig. 11 are available experimental data[34] along with the previous PIMC results[2] and new estimates obtained in the present study, extrapolated to the thermodynamic limit as explained above. With new technology we substantially reduce theoretical uncertainties on predictions of n_o at the SVP.

We conclude by mentioning that we have also obtained estimates for all other standard thermodynamic quantities, such as the kinetic energy, pair correlation function etc. Our data are generally consistent with those of existing calculations; specifically, our T=1 K results are indistinguishable, within statistical uncertainties, from those yielded by numerically exact ground state methods (see, e.g., Ref. 35).

VII. DISCUSSION AND CONCLUSIONS

We have introduced a new Worm algorithm, affording an accurate PIMC study of strongly correlated Bose systems. Illustrative results of numerical simulations of the superfluid transition in liquid ^{4}He have been presented, for system sizes two orders of magnitude larger than what is accessible to conventional PIMC. It should be stressed that such an advance cannot be simply attributed to the availability of faster computing facilities than back in the days when the first PIMC simulations of liquid ^{4}He were carried out. Rather, the WA decisively overcomes the most important limitation of conventional PIMC, namely the exponential inefficiency with which long permutation cycles are sampled, in the thermodynamic limit (a limitation acknowledged by practitioners of PIMC[6]).

We have also described a procedure, based on ideas of Diagrammatic Monte Carlo, which allows one to enhance significantly the scalability of the computational scheme, without compromising on the accuracy of the calculation.

The new methodology has already been applied to the study of the supersolid phase of helium,[12] for which access to large system sizes is crucial; it can also be expected to have broad impact on a wide variety of strongly correlated quantum many-body systems. It should be mentioned, that the efficiency with which long permutation cycles can be sampled using the WA, also significantly impacts the convergence of calculations of the superfluid properties of *finite* systems, such as quantum clusters.[13]

There are other advantages to this new method, chiefly the fact that it is fully grand canonical, and that allows for the calculation of the Matsubara Green function, a quantity that can not e computed with any other existing QMC technique (in continuous space). An immediate application of these last two aspects, is the calculation of chemical potentials and excitation gaps. Consider, for instance, the calculation of the chemical potential at the liquid-solid transition line at low temperature, $\mu_\circ$. The study of $G(k=0,\tau)$ in the solid phase can be found in Ref. 36.

The value of $\mu_\circ$ can be determined from the $n(\mu)$ curve and known freezing density for the liquid which is at $n = 0.02599$ Å^{-3}. In Fig. 12 we show data points for four values of the chemical potential and the position of the freezing density. All simulations were performed at $T = 0.25$ K, and with the particle number $N \approx 800$. Apart from average density we also calculated statistics of particle number fluctuations to obtain the compressibility of the system from $\kappa = dn/d\mu = \langle (N - \langle N \rangle)^2 \rangle / TV$. It provides an independent check for consistency and convergence of the data. In Fig. 12 the slope of the solid line is obtained from the average value of κ for all data points shown. From this set of data we deduce that the critical value of the chemical potential as

$$\mu_o = 0.06 \pm 0.04 \, . \tag{7.1}$$

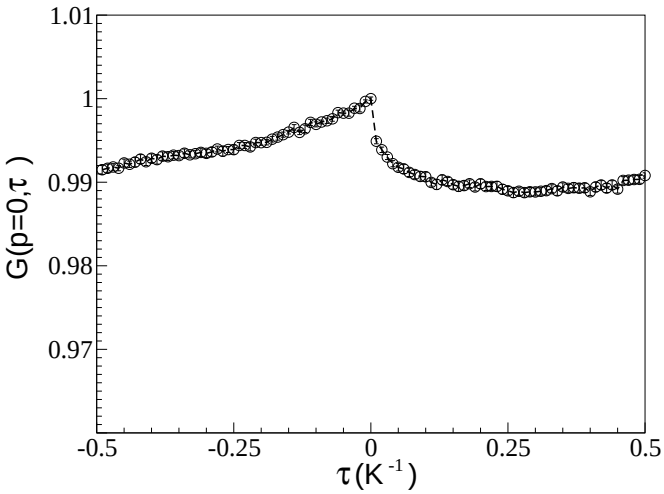

FIG. 13: Zero-momentum Green function for the superfluid state of $N \approx 1000$ atoms at $T = 1$ K, $\mu = -7.35$ K, and density $n = 0.02184$ Å^{-3} . It is normalized to unity at the origin. Note the small vertical scale: The τ-dependence is a finite-size effect.

Though one can deduce this parameter from the ground state energy as a function of particle number using $\mu = dE/dN \approx E(N+1) - E(N)$, such simulations can not be performed for large system sizes with accuracy significantly better then few K.

The zero-momentum Matsubara Green function $G(k = 0, \tau)$ for the superfluid state at $T = 1$ is shown in Fig. 13. In the macroscopic limit, $G(k = 0, \tau)$ is τ-independent, being equal to the total number of condensate particles. We show this plot to support our previous claim that in the superfluid state the two worm ends perform a random walk on large distances, and come close within the reach of the *Close* and *Remove* updates once per sweep.

VIII. ACKNOWLEDGMENTS

This work was supported by the National Aero and Space Administration grant NAG3-2870, the National Science Foundation under Grants Nos. PHY-0426881, NSF PHY-0456261, by the Sloan Foundation, and by the Natural Science and Engineering Research Council of Canada under grant G121210893. NP gratefully acknowledges hospitality and support from the Pacific Institute of Theoretical Physics, Vancouver (BC).

[1] D. M. Ceperley and E. L. Pollock, Phys. Rev. Lett. **56**, 351 (1986).

[2] D. M. Ceperley, Rev. Mod. Phys. **67**, 279 (1995).

[3] See, for instance, D. M. Ceperley in *Monte Carlo and Molecular Dynamics of Condensed Matter Systems*, Ed. K. Binder and G. Ciccotti, Editrice Compositori (Bologna, Italy, 1996).

[4] See, for instance, A. Brenner, *Physics Today*, October 1996, p. 24.

[5] E. L. Pollock and D. M. Ceperley, Phys. Rev. B **36**, 8343 (1987).

[6] See, for instance, B. Bernu and D. M. Ceperley, Phys. Rev. Lett. **95**, 155303 (2004).

[7] E.L. Pollock and K.J. Runge, Phys. Rev. B **46**, 3535 (1992).

[8] N. V. Prokof'ev, B. V. Svistunov, and I. S. Tupitsyn, Phys. Lett. A **238**, 253 (1998); Sov. Phys. JETP **87**, 310 (1998).

[9] N. V. Prokof'ev and B. V. Svistunov, Phys. Rev. Lett. **92**, 015703 (2004).

[10] N. V. Prokof'ev and B. V. Svistunov Phys. Rev. Lett. **87**, 160601 (2001).

[11] M. Boninsegni, N. Prokof'ev, and B. Svistunov, Phys. Rev. Lett. **96**, 070601 (2006).

[12] M. Boninsegni, N. V. Prokof'ev and B. V. Svistunov, Phys. Rev. Lett. **96**, 105301 (2006).

[13] F. Mezzacapo and M. Boninsegni, Phys. Rev. Lett. **97**, 045301 (2006).

[14] N. V. Prokof'ev and B. V. Svistunov, Phys. Rev. Lett. **81**, 2514 (1998).

[15] The WA can be applied to Fermi systems as well; however it will be affected by the *sign* problem. Although we do not discuss the fermion problem here, we note that approximate schemes such as the "fixed-node approximation" (see, for instance, Ref. 3) can be easily incorporated in the WA.

[16] Note that this assumption on the potential is made for simplicity only; the applicability of the WA does not depend on it, i.e., more general interactions can be studied without altering the computational scheme in any significant way.

[17] Using standard importance sampling, one may control statistics of particle number fluctuations, and perform canonical ensemble measurements.

[18] N. A. Metropolis, A. W. Rosenbluth, M. N. Rosenbluth, A. Teller and E. Teller, J. Chem. Phys. **21**, 1087 (1953).

[19] Since balance equation deals only with *accepted* moves, one can propose a move without *a priori* checking that the current configuration is consistent with the proposal.—If it is not, the move is automatically rejected after the proposal, with no calculation needed.

[20] See, for instance, M. P. Allen and D, J. Tildesley, *Computer Simulation of Liquids*, Oxford University Press (1987).

[21] The specific definition of "nearest neighbor" is not relevant for the generic description of the move.

[22] A. S. Mishchenko, N. Nagaosa, N. V. Prokof'ev, A. Sakamoto, and B. V. Svistunov, Phys. Rev. B **62**, 6317 (2000).

[23] S. A. Chin, Phys. Lett. A **226**, 344 (1997).

[24] R. A. Aziz, V. P. S. Nain, J. S. Carley, W. L. Taylor and G. T. McConville, J. Chem. Phys. **70**, 4330 (1979).

[25] D. M. Ceperley and E. L. Pollock, Phys. Rev. B **39**, 2084 (1989).

[26] The largest system size for which calculations of superfluid properties of helium films have been carried out using conventional PIMC, is, to date N=36. M. Boninsegni, M. W. Cole and F. Toigo, Phys. Rev. Lett. **87**, 2002 (1999).

[27] J. M. Kosterlitz and D. J. Thouless, Prog. Low Temp. Phys. **VIIB**, 371 (1978).

[28] S. Moroni and M. Boninsegni, J. Low Temp. Phys. **136**, 129 (2004).

[29] K. Binder, Phys. Rev. Lett. **47**, 693 (1981); W.H. Press, S.A. Teukolsky, W.T. Vetterling, and B.P. Flannery, *Numerical Recipes in C*, 2nd ed, Cambridge, 1992.

[30] M. Campostrini, M. Hasenbusch, A. Pelissetto, P. Rossi, and E. Vicari, Phys. Rev. B **63**, 214503 (2001); E. Burovski, J. Machta, N.V. Prokof'ev, and B.V. Svistunov, cond-mat/0507352; M. Campostrini, M. Hasenbusch, A. Pelissetto, and E. Vicari, cond-mat/0605083.

[31] E. L. Pollock and D. M. Ceperley, Phys. Rev. B **36**, 8343 (1987).

[32] M.-C. Cha, M.P.A. Fisher, S.M. Girvin, M. Wallin, and A.P. Young, Phys. Rev. B **44**, 6883 (1991).

[33] See, for instance, S. Moroni, F. Pederiva, S. Fantoni and M. Boninsegni, Phys. Rev. Lett. **84**, 2650 (2000), and references therein.

[34] H. R. Glyde, R. T. Azuah and W. G. Stirling, Phys. Rev. B **62**, 14337 (2000).

[35] J. E. Cuervo, P.-N. Roy and M. Boninsegni, J. Chem. Phys. **122**, 114504 (2005).

[36] M. Boninsegni, A. B. Kuklov, L. Pollet, N. V. Prokof'ev, B. V. Svistunov, M. Troyer, Phys. Rev. Lett. **97**, 080401 (2006).